








Spatial Distribution of AIO in a High-mass Protostar Candidate Orion Source I

Shogo Tachibana^{1,2} , Takafumi Kamizuka³, Tomoya Hirota^{4,5} , Nami Sakai⁶ , Yoko Oya⁷ , Aki Takigawa⁸ , and Satoshi Yamamoto⁷

¹UTokyo Organization for Planetary and Space Science, the University of Tokyo, 7-3-1 Hongo, Tokyo 113-0033, Japan; tachi@eps.s.u-tokyo.ac.jp

²Institute of Space and Astronautical Science, Japan Aerospace Exploration Agency, 3-1-1 Yoshinodai, Sagami-hara, Kanagawa 252-5210, Japan

³Institute of Astronomy, The University of Tokyo, 2-21-1 Osawa, Mitaka, Tokyo 181-0015, Japan

⁴Mizusawa VLBI Observatory, National Astronomical Observatory of Japan, Osawa 2-21-1, Mitaka, Tokyo 181-8588, Japan

⁵Department of Astronomical Sciences, SOKENDAI (The Graduate University for Advanced Studies), Osawa 2-21-1, Mitaka, Tokyo 181-8588, Japan

⁶RIKEN Cluster for Pioneering Research (CPR), 2-1, Hirosawa, Wako, Saitama 351-0198, Japan

⁷Department of Physics, The University of Tokyo, 7-3-1 Hongo, Tokyo 113-0033, Japan

⁸The Hakubi Center for Advanced Research/Division of Earth and Planetary Sciences, Kyoto University, Kitashirakawa Oiwake-cho, Sakyo, Kyoto 606-8502, Japan

Received 2019 March 17; revised 2019 April 3; accepted 2019 April 4; published 2019 April 24

Abstract

High-temperature molecular gas containing metallic elements is potentially a good probe to trace the kinematics/dynamics of circumstellar disks, and its presence in circumstellar disks around young stellar objects (YSOs) may also give some insights into formation processes of high-temperature meteoritic components formed in the Sun's protoplanetary disk. The Orion Kleimann–Low (KL) region is the most famous and nearest massive star formation site, and has been extensively studied since the 1970s. The KL region harbors a candidate high-mass YSO, Source I, which has a hot circumstellar rotating gas disk emanating a magnetocentrifugal wind of SiO. In this study, we report spatially resolved distributions of aluminum monoxide (AIO) emission lines at 497 and 650 GHz in the rotating outflow of Orion Source I based on subarcsecond observations obtained by the Atacama Large Millimeter/Submillimeter Array for the first time in star-forming regions. These AIO emissions are detected only at the base of the outflow as the high excitation line of H₂O in spite of their low excitation temperatures. The limited distribution of AIO to the launching point of the outflow indicates that AIO is not in the gas phase in the outer part of the outflow lobes away from the disk surface, which could be attributed to recondensation of AIO as dust due to its refractory nature.

Key words: ISM: individual objects (Orion Source I) – radio lines: stars – stars: formation – stars: massive

1. Introduction

High-temperature molecular gas containing metallic elements can be used as a probe to trace the kinematics/dynamics of circumstellar disks (e.g., Plambeck & Wright 2016; Hirota et al. 2017; Ginsburg et al. 2018, 2019; Kim et al. 2019). The Orion Kleimann–Low (KL) region is the nearest active massive star formation site (e.g., 418 pc, Kim et al. 2008) and has been extensively studied for high-mass star formation (e.g., Zuckerman et al. 1976; Genzel et al. 1978; Hirota et al. 2012, 2015, 2016, 2017; Plambeck & Wright 2016; Ginsburg et al. 2018, 2019). Hirota et al. (2017) observed a rotational transition of silicon monoxide (Si¹⁸O, $J = 12-11$) around Orion Source I, which is a young stellar object (YSO) candidate ($5-7 M_{\odot}$; Plambeck & Wright 2016; $15 M_{\odot}$; Ginsburg et al. 2018) located in the Orion KL region, using the Atacama Large Millimeter/submillimeter Array (ALMA). They found that Si¹⁸O molecules are ejected as rotating outflow (10 km s^{-1}) from >10 au from the central object, which should be driven by the magnetocentrifugal disk wind launched by the high-mass YSO candidate and should contribute to the angular momentum transfer of the system. Ginsburg et al. (2018) observed SiO $\nu = 0$ $J = 5-4$ and ²⁹SiO $J = 5-4$ emissions with similar spatial distributions to that of Si¹⁸O $J = 12-11$, which also indicates the presence of a rotating, expanding outflow. Kim et al. (2019) detected the emission lines of SiO in

Orion Source I (²⁹SiO $\nu = 2$ $J = 11-10$, SiO $\nu = 2$ $J = 10-9$, and SiO $\nu = 4$ $J = 11-10$), among which the detection of the SiO $\nu = 4$ line was the first in star-forming regions. The SiO $\nu = 2$ $J = 10-9$ emission was detected in the rotating outflow as the Si¹⁸O $J = 12-11$ line (Hirota et al. 2017), while the distributions of ²⁹SiO $\nu = 2$ $J = 11-10$ and SiO $\nu = 4$ $J = 11-10$ lines are limited to the base of the outflow. Ginsburg et al. (2019) recently made the first detection of NaCl, KCl, and their isotopologues with ³⁷Cl and ⁴¹K in the base of the outflow of Orion Source I, which could be useful molecules to study the kinematics and physical conditions of the disk surrounding Orion Source I.

Aluminum monoxide (AIO) is a molecule that can be present in the gas phase at high temperature (e.g., >1650 K at total pressure of 10^{-5} bar in a gas of solar composition; Ebel 2006), and is also potentially a good tracer of the kinematics of high-temperature region around YSOs. There has been no definitive detection of AIO in the star-forming regions although tentative detection of AIO emissions at 229.7 and 344.4 GHz is claimed in Orion Source I (Ginsburg et al. 2019). The molecule has been observed around oxygen-rich evolved stars (Tenenbaum & Ziurys 2009; Kamiński et al. 2016; De Beck et al. 2017; Decin et al. 2017; Takigawa et al. 2017). The spatially resolved observation of AIO around W Hya with ALMA showed that AIO is present only at <3 stellar radii with a consistent distribution with dust, while ²⁹SiO is present in the accelerated stellar outflow beyond 5 stellar radii without severe depletion inside <3 stellar radii (Takigawa et al. 2017). This indicates that AIO form aluminum oxide dust around W Hya and that the aluminum oxide dust contributes to the wind acceleration,



Original content from this work may be used under the terms of the [Creative Commons Attribution 3.0 licence](https://creativecommons.org/licenses/by/3.0/). Any further distribution of this work must maintain attribution to the author(s) and the title of the work, journal citation and DOI.

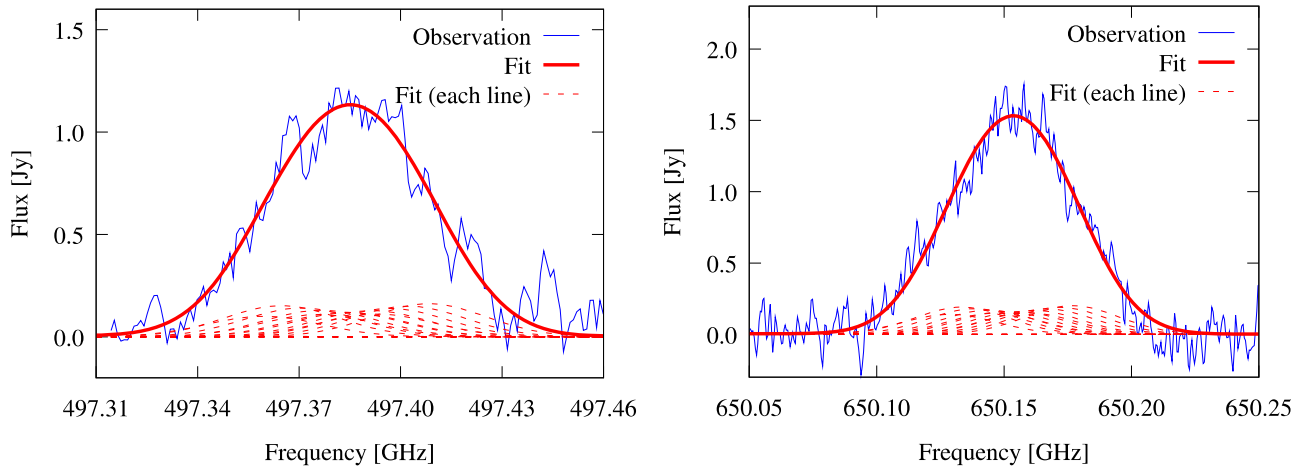


Figure 1. Emission peaks at 497 and 650 GHz observed in Orion Source I. The observed spectra (blue solid curves) are measured in the regions with distances less than 0.25 and 0.4 arcsec from Orion Source I for 497 and 650 GHz data, respectively. Red solid curves are simulated spectra of AIO at 497 and 650 GHz with systemic velocities of 3.6 ± 0.3 and 4.6 ± 0.1 km s⁻¹, and velocity widths of 24.1 ± 0.9 and 20.0 ± 0.4 km s⁻¹ (FWHM) for each hyperfine structure (shown in red dashed curves).

which prevents the efficient formation of silicate dust around W Hya due to abrupt decrease of the gas density and explains the aluminum oxide dust-enriched nature of W Hya (Takigawa et al. 2017).

Aluminum monoxide is a key molecule in the formation of most refractory solids in a gas of solar composition. In outflows of oxygen-rich AGB stars, AIO form the first dust as aluminum oxide including corundum (α -Al₂O₃; Takigawa et al. 2015, 2017), and such circumstellar corundum grains formed prior to the Sun’s birth are found as a rare but important component (presolar grains) in pristine undifferentiated chondrites (e.g., Takigawa et al. 2014, 2018). Chondrites also contain inclusions consisting of minerals enriched in refractory elements (e.g., Ca, Al, and Ti). Such Ca- and Al-rich inclusions (CAIs) are the oldest solid objects formed in the solar system (e.g., Connelly et al. 2012). The chemistry, mineralogy, and petrology of CAIs strongly suggest their high-temperature origin in the very early stage of disk evolution, but it has been under debate where and how CAIs formed in the early solar system. The observation of AIO around YSOs may provide a new insight into the formation of the oldest high-temperature solid objects in the early solar system.

In this study we analyzed the ALMA observation data for Orion Source I in Orion KL to search for AIO molecules and report the spatially resolved detection of AIO around Orion Source I for the first time.

2. Data Reduction

We used the ALMA observation data of Orion Source I obtained in Cycle 1 (2012.1.00123.S) and Cycle 2 projects (2013.1.00048.S). The Band 8 data in the Cycle 2 observation and the Band 9 data in the Cycle 1 observation were used for investigating AIO emissions at 497 and 650 GHz, respectively. The data were reduced following the procedure described in Hirota et al. (2017). The reduction was processed with the Common Astronomy Software Applications software (<https://casa.nrao.edu/>). We first applied the self-calibration process to obtain better quality data. Both phase and amplitude solutions were derived from the continuum image of the target by using “gaincal” and “clean” tasks. The channels to make the continuum image were defined by checking by eye the

spectrum derived from the dirty image. After applying the phase and amplitude solutions, continuum emission was subtracted with the “uvcontsub” task. The line images were synthesized from these continuum-subtracted data through the “clean” process with uniform weighting. The synthesized beam was $122 \text{ mas} \times 97 \text{ mas}$ ($50 \text{ au} \times 40 \text{ au}$) with a position angle of 85° for the 497 GHz data, and that for the 650 GHz data was $180 \text{ mas} \times 145 \text{ mas}$ ($75 \text{ au} \times 60 \text{ au}$) with a position angle of -34° .

3. Results

We found broad emission features at 497 and 650 GHz (Figure 1), one of which (650 GHz) was assigned as an unidentified peak by Plambeck & Wright (2016). The lines observed at 497 and 650 GHz are compared with the AIO ($N = 13-12$ and $17-16$) lines (Pickett et al. 1998) (Figure 1). The AIO emission peaks have hyperfine structures, and we applied a line-of-sight velocity with the Gaussian velocity dispersion to each hyperfine structure of the AIO emission. The relative intensities of hyperfine structures in the local thermal equilibrium at 300 K (Pickett et al. 1998) were used for the calculation. The peaks at 497 and 650 GHz can be well reproduced with the line-of-sight velocities of 3.6 ± 0.3 and 4.6 ± 0.1 km s⁻¹ and the velocity widths (FWHM) of 24.1 ± 0.9 and 20.0 ± 0.4 km s⁻¹ for the Gaussian dispersion, respectively. The line-of-sight velocities of $3.6-4.6$ km s⁻¹ are consistent with those of other molecules (e.g., SO, SO₂, SiS, SiO, H₂O, and alkali halides) observed for Orion Source I (Plambeck & Wright 2016; Hirota et al. 2017; Ginsburg et al. 2019; Kim et al. 2019). The integrated intensities of the 497 and 650 GHz emissions are $(7.0 \pm 0.1) \times 10^{-19}$ and $(9.3 \pm 0.1) \times 10^{-19}$ W m⁻², respectively. The total numbers of emitting AIO molecules can be derived by assuming spherical symmetry, distance (418 pc; Kim et al. 2008), and temperature (300 K). They were $(6.25 \pm 0.19) \times 10^{45}$ and $(3.34 \pm 0.06) \times 10^{45}$ molecules, corresponding to $(2.24 \pm 0.07) \times 10^{-10}$ and $(1.20 \pm 0.02) \times 10^{-10} M_\odot$, for the 497 and 650 GHz lines, respectively. These numbers could be several times higher if higher temperature is assumed.

The integrated flux (moment 0) maps of the two emission features show that they are localized near the central object,

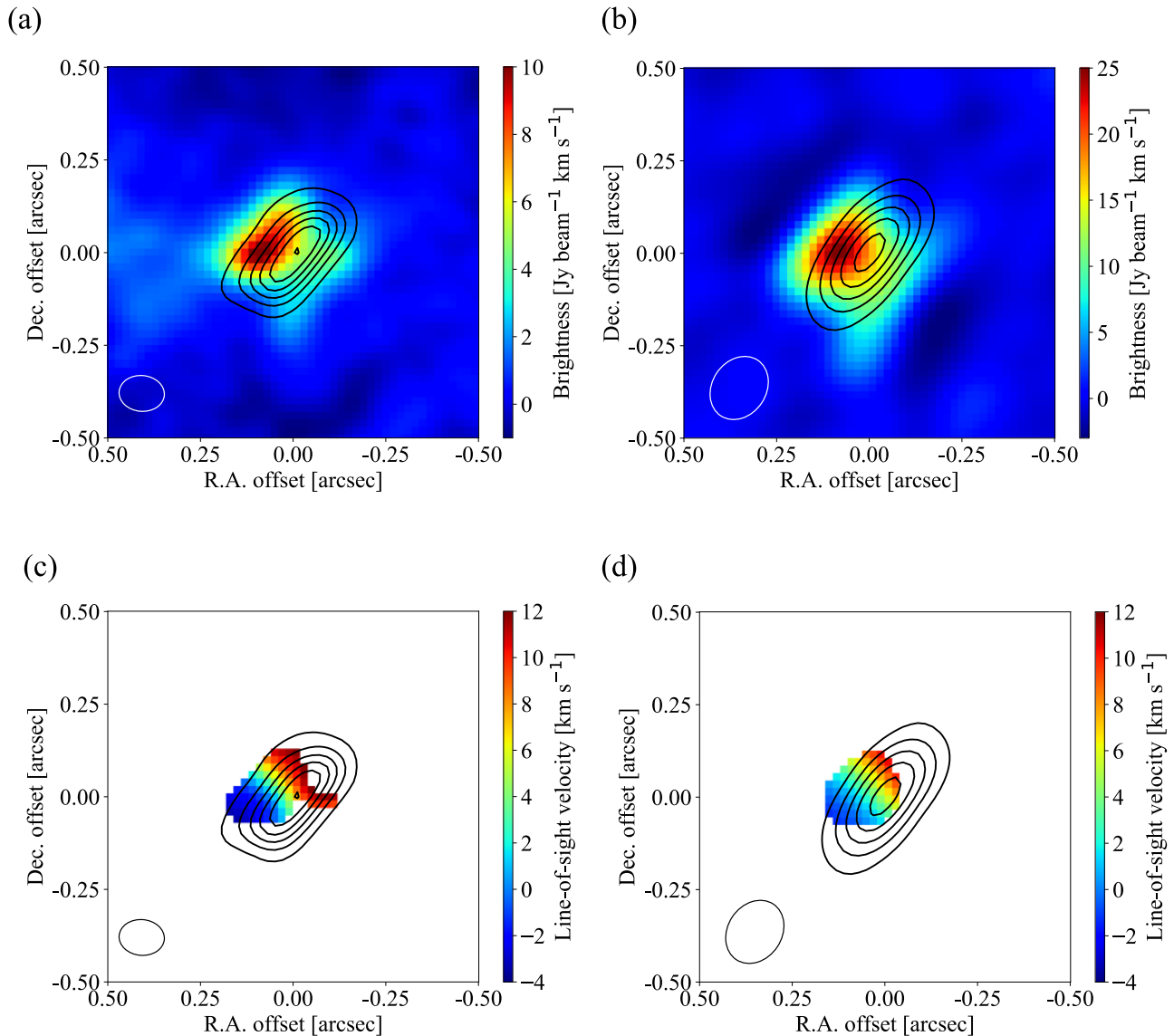


Figure 2. Moment 0 maps of AIO emissions at (a) 497 and (b) 650 GHz and line-of-sight velocity maps of (c) 497 and (d) 650 GHz. Synthesized beam sizes are shown at the bottom-left corner of each panel. The continuums at 497 and 650 GHz are also shown as black contours in the maps for 497 and 650 GHz, respectively. Contour levels are 0.1, 0.2, ..., 0.6 and 0.3, 0.6, ..., 1.5 Jy beam⁻¹ for 497 and 650 GHz, respectively. Line-of-sight velocities are derived using data with >10 times the root-mean-square (r.m.s.) noise level. The r.m.s. noise levels are 21 and 59 mJy beam⁻¹ for 497 and 650 GHz, respectively.

especially along the disk plane around the central object as the emissions of H₂O (463 GHz; Hirota et al. 2017), ²⁹SiO $\nu = 2$ $J = 11-10$, SiO $\nu = 4$ $J = 11-10$ (Kim et al. 2019), and alkali halides (Ginsburg et al. 2019; Figures 2(a) and (b)). The line-of-sight velocity distributions of the 497 and 650 GHz emissions (Figures 2(c) and (d)), which were derived by applying the same fitting analysis as shown in Figure 1 to the spectrum of each pixel, are also consistent with the maps of intensity weighted velocity fields of gas species observed nearby the launching point of the outflow (Hirota et al. 2017; Ginsburg et al. 2019; Kim et al. 2019).

The velocity widths of 20–24 km s⁻¹ (Figure 1) represent the velocity variation of rotating gas along the line-of-sight direction, and both lines show a line-of-sight velocity of around 5.5 km s⁻¹ in the central region, where the systemic velocity of the object should be observed without a significant effect from the rotating motion. The derived velocities of ~ 5.5 km s⁻¹ are close to the systemic velocity of Orion Source I (Plambeck et al. 1990). This result consolidates our conclusion that the

497 and 650 GHz emissions originate from AIO molecules. We note that the 497 and 650 GHz emissions are not contaminated from complex organic molecules (COMs) observed in the Orion-KL region (Pagani et al. 2017). The 497 and 650 GHz emissions have broader velocity widths (Figure 1) and are present only in the compact region around Orion Source I (Figure 2), which are not the characteristics of COMs (velocity widths $\sim 3-5$ km s⁻¹) in this region.

These lines of evidence strongly suggest that AIO is the molecule emitting at 497 and 650 GHz and that AIO is present in the launching point of outflow from the circumstellar rotating disk of Orion Source I. The report of AIO emission lines at 229.7 and 344.4 GHz in Orion Source I (Ginsburg et al. 2019) also corroborates the conclusion in this study.

4. Discussion

The distribution of AIO is limited to the base of the rotating outflow from the disk as H₂O at 463 GHz ($\nu_2 = 1$,

$J_{Ka,Kc} = 4_{2,2}-3_{3,1}$) and the rotating outflow nearby the launching region (Figure 2), while the Si¹⁸O $J = 12-11$ emission line (Hirota et al. 2017) are observed in an expanding rotating outflow (10 km s⁻¹). The lower energy state of H₂O at 463 GHz is 2744 K, while those of Si¹⁸O $J = 12-11$ is 128 K. The high excitation line of H₂O is therefore observed only at the base of the outflow.

The upper state energies of AIO lines at 497 and 650 GHz are ~ 167 and ~ 281 K, respectively (Pickett et al. 1998), and are much lower than that of H₂O at 463 GHz. The AIO emissions could thus be detected in the wide range of the outflow from the disk as Si¹⁸O $J = 12-11$ if AIO molecules were present in the gas phase with the solar Al/Si ratio of ~ 0.08 (Lodders 2003). The limited distribution of AIO emissions to the base of the outflow (Figure 2) indicates that AIO molecules are not present in the gas phase, which is likely due to its refractory nature. Aluminum monoxide molecules condense as refractory dust such as corundum (Al₂O₃) and hibonite (CaAl₁₂O₁₉) that are more refractory than silicate dust. Aluminum monoxide may thus not be present in the gas phase in the expanding outflow due to recondensation of refractory dust as discussed for alkali halides (Ginsburg et al. 2019), while SiO molecules sublimated from silicate dust are present in the gas phase in the outflow.

We note that the AIO emissions distribute to a greater extent in the outflow than alkali halides, which are observed only just above the continuum disk (Ginsburg et al. 2019), not significantly exceeding the contour of 0.3 Jy beam⁻¹ for the 497 GHz continuum in Figure 2(a). This implies that AIO and alkali halides behave differently in the outflow, and that alkali halides may condense as solid more effectively than AIO. Gas phase reactions that consume alkali halide molecules or dissociation of alkali halide molecules could also be responsible for their limited distributions (Ginsburg et al. 2019). Asymmetric distribution of AIO is also a notable feature, where the emissions are stronger in the northeast than in the southwest (Figure 2). The asymmetric distribution is suggested for the SiO $\nu = 4$ line (Kim et al. 2019), but the degree of asymmetry of AIO distribution appears to be larger than SiO, H₂O, and alkali halides observed in the outflow (e.g., Hirota et al. 2017; Ginsburg et al. 2019). Further investigation, including observation of multiple molecules with different chemical characteristics, is required to understand the chemical processes in the outflow and the origin of the asymmetric distribution of AIO.





The detection of AIO around the central object of Orion Source I will provide further opportunities to study the structure, kinematics, and dynamics of the high-temperature inner region of the circumstellar disk of Orion Source I. The hot nature of the disk around the embedded massive protostar suggests that solid objects that are enriched in refractory elements, similar to the oldest solar system solid, could form in the disk. Further observations of high-temperature metal-bearing gas molecules in the disk around YSOs could link the high-temperature CAI formation event occurred in the early solar system to the star formation and subsequent planetary formation processes, which is a key research topic in meteoritics. We note that Orion Source I could be an evolved

star in the very early stage of the protoplanetary nebula phase (Báez-Rubio et al. 2018), peculiarly located in the active massive-star formation site. If this is the case, the detection of circumstellar AIO molecules would provide insights into dust formation and possibly the kinematics of mass loss as in the case of W Hya (Takigawa et al. 2017).

We thank the anonymous referee for a constructive review. This paper makes use of the following ALMA data: ADS/JAO.ALMA#2012.1.00123.S and #2013.1.00048.S. ALMA is a partnership of ESO (representing its member states), NSF (USA) and NINS (Japan), together with NRC (Canada), NSC and ASIAA (Taiwan), and KASI (Republic of Korea), in cooperation with the Republic of Chile. The Joint ALMA Observatory is operated by ESO, AUI/NRAO and NAOJ. S.T., N.S., T.H., and S.Y. are financially supported by MEXT Grant-in-Aid for Scientific Research on Innovative Areas (25108002 and 25108005). T.H. is financially supported by the MEXT/JSPS KAKENHI grant No. 17K05398. Data analysis was in part carried out on the common use data analysis computer system at the Astronomy Data Center, ADC, of NAOJ.

Facility: ALMA.

ORCID iDs

Shogo Tachibana  <https://orcid.org/0000-0002-4603-9440>
 Tomoya Hirota  <https://orcid.org/0000-0003-1659-095X>
 Nami Sakai  <https://orcid.org/0000-0002-3297-4497>
 Yoko Oya  <https://orcid.org/0000-0002-0197-8751>
 Aki Takigawa  <https://orcid.org/0000-0002-0649-6997>

References

- Báez-Rubio, A., Jiménez-Serra, I., Martín-Pintado, J., Zhang, Q., & Curiel, S. 2018, *ApJ*, **853**, 4
- Connelly, J. N., Bizzarro, M., Krot, A. N., et al. 2012, *Sci*, **338**, 651
- De Beck, E., Decin, L., Ramstedt, S., et al. 2017, *A&A*, **598**, A53
- Decin, L., Richards, A. M. S., Waters, L. B. F. M., et al. 2017, *A&A*, **608**, A55
- Ebel, D. 2006, in *Meteorites and the Early Solar System II*, ed. D. S. Lauretta (Tucson, AZ: Univ. Arizona), 253
- Genzel, R., Downes, D., Moran, J. M., et al. 1978, *A&A*, **66**, 13
- Ginsburg, A., Bally, J., Goddi, C., et al. 2018, *ApJ*, **860**, 119
- Ginsburg, A., McGuire, B., Plambeck, R. L., et al. 2019, *ApJ*, **872**, 54
- Hirota, T., Kim, M. K., & Honma, M. 2012, *ApJL*, **757**, L1
- Hirota, T., Kim, M. K., Kurono, Y., & Honma, M. 2015, *ApJ*, **801**, 82
- Hirota, T., Machida, M. N., Matsushita, Y., et al. 2016, *ApJ*, **833**, 238
- Hirota, T., Machida, M. N., Matsushita, Y., et al. 2017, *NatAs*, **1**, 0146
- Kamiński, T., Wong, K. T., Schmidt, M. R., et al. 2016, *A&A*, **592**, A42
- Kim, M. K., Hirota, T., Honma, M., et al. 2008, *PASJ*, **60**, 991
- Kim, M. K., Hirota, T., Machida, M. N., et al. 2019, *ApJ*, **872**, 64
- Lodders, K. 2003, *ApJ*, **591**, 1220
- Pagani, L., Favre, C., Goldsmith, P. F., et al. 2017, *A&A*, **604**, A32
- Pickett, H. M., Poynter, R. L., Cohen, E. A., et al. 1998, *JQSRT*, **60**, 883
- Plambeck, R. L., & Wright, M. C. H. 2016, *ApJ*, **833**, 219
- Plambeck, R. L., Wright, M. C. H., & Carlstrom, J. E. 1990, *ApJ*, **348**, L65
- Takigawa, A., Kamizuka, T., Tachibana, S., & Yamamura, I. 2017, *SciA*, **3**, eao2149
- Takigawa, A., Stroud, R. M., Nittler, L. R., et al. 2018, *ApJL*, **862**, L13
- Takigawa, A., Tachibana, S., Huss, G. R., et al. 2014, *GeCoA*, **124**, 309
- Takigawa, A., Tachibana, S., Nagahara, H., & Ozawa, K. 2015, *ApJS*, **218**, 2
- Tenenbaum, E. D., & Ziurys, L. M. 2009, *ApJ*, **694**, L59
- Zuckerman, B., Kuiper, T. B. H., & Rodriguez Kuiper, E. N. 1976, *ApJL*, **209**, L137